universe

IMPACT FACTOR 2.5

CITESCORE 4.3

Article

Exploring the Enigma of Particle Dynamics and Plasma Lensing Using Einstein–Euler–Heisenberg Black Hole Geometry

Allah Ditta, Raja Sikander Mehmood, Muhammad Fiaz, Bismillah Bibi, Sana Deen, Rimsha Jaffar and Asif Mahmood

Topic Collection

Open Questions in Black Hole Physics

Edited by

Dr. Gonzalo J. Olmo and Dr. Diego Rubiera-Garcia

MDPI

https://doi.org/10.3390/universe11010019

universe

MDPI

Article

Exploring the Enigma of Particle Dynamics and Plasma Lensing Using Einstein–Euler–Heisenberg Black Hole Geometry

Allah Ditta [1,2,*], Raja Sikander Mehmood [3], Muhammad Fiaz [3], Bismillah Bibi [3], Sana Deen [3], Rimsha Jaffar [3] and Asif Mahmood [4]

[1] Department of Mathematics, School of Science, University of Management and Technology, Lahore 54000, Pakistan
[2] Research Center of Astrophysics and Cosmology, Khazar University, 41 Mehseti Street, Baku AZ1096, Azerbaijan
[3] Department of Mathematics, Government Graduate College Sahiwal, Sahiwal 46001, Pakistan; sikander.mehmood@gpgcs.edu.pk (R.S.M.); muhammadfiaz57000@gmail.com (M.F.); bismillahghulamabbas@gmail.com (B.B.); deensana53@gmail.com (S.D.); wasimjafar47@gmail.com (R.J.)
[4] College of Engineering, Chemical Engineering Department, King Saud University, Riyadh 11421, Saudi Arabia; ahayat@ksu.edu.sa
* Correspondence: allahditta@umt.edu.pk or mradshahid01@gmail.com

Abstract: The unified Einstein–Euler–Heisenberg theory is utilized to investigate the particle motion and weak gravitational lensing characteristics of black holes. This black hole solution is developed using spherically symmetric possessing electric and magnetic charges. Quantum electrodynamics corrections reveal a screening effect for BH electric charges and paramagnetic impacts on magnetic charges. We analyzed the motion of massive as well as massless particles by studying their effective potential, event horizon, photon orbit and inner circular orbit. It was demonstrated that magnetic and electric fields of spherically symmetric black holes have significant impact. Then, we also delve to study the weak gravitational lensing phenomenon. A comprehensive approach was employed to investigate this phenomenon and explore the angle of deflection of light rays near magnetically and electrically charged black holes.

Keywords: Einstein–Euler–Heisenberg black hole; non-linear electrodynamics; particle dynamics; weak gravitational lensing

Academic Editors: Gonzalo J. Olmo and Diego Rubiera-Garcia

Received: 4 December 2024
Revised: 8 January 2025
Accepted: 9 January 2025
Published: 13 January 2025

Citation: Ditta, A.; Mehmood, R.S.; Fiaz, M.; Bibi, B.; Deen, S.; Jaffar, R.; Mahmood, A. Exploring the Enigma of Particle Dynamics and Plasma Lensing Using Einstein–Euler–Heisenberg Black Hole Geometry. *Universe* **2025**, *11*, 19. https://doi.org/10.3390/universe11010019

1. Introduction

General Relativity (GR) was introduced in 1915, and has been examined by several experiments and observations. Recent findings of gravitational waves in space [1] and the shadow of M87 [2] offer an intense field domain test of GR, whereas solar system tests [3] are considered weak field regime tests. However, General Relativity (GR) falls short in understanding the singularity that occurs during the collapse associated with the acceleration of cosmic expansion, the rotation curves of galaxies, and alignment with the theory of quantum fields. To address such shortfalls, one can either employ other gravity theories or break GR's symmetry. For several years, researchers in physics have been captivated by the electromagnetic interactions with nonlinear behavior of the Reissner's solution to Einstein and Maxwell's equations. Gravitational Born–Infeld (BI) theory [4] is the widely recognized example. In the 1930s, gravitational nonlinear electrodynamics was researched [5,6]. The revelation that string theory and D-brane physics generate Lagrangians resembling both Born–Infeld theories (Abelian and non-Abelian) in the environment of their regime low energy (as referenced in [7–9]) has sparked a renewed fascination with these nonlinear

operations. There exist black hole (BH) solutions that are static, spherically symmetric, and asymptotically flat (as discussed in [10,11]).

Black holes in Born–Infeld that have a universal constant have been researched in many aspects [12,13]. In recent decades, various nonlinear electrodynamics theories have been recommended to clarify static and spherically symmetric structures, including those with a gauge invariant's general function [14–17], a logarithmic Maxwell invariant's function [18], and a nonlinear Langrangian [19], which is generalized and can lead one to the Lagrangian of BI, and is the limit of the weak-field of the Lagrangian of the Einstein–Euler–Heisenberg theory [20]. Within Ref. [21], the gravity of BHs (spherically symmetric and static) was examined alongside electrodynamics, which is a nonlinear limiting of the weakfield of the Lagrangian of the Heisenberg–Euler–Schwinger model. Attempts to acquire BH solutions that are spherically symmetric and regularly (singularity free) static using gravitational electrodynamics that is nonlinear have been studied [22–26]. References [27,28] provide detailed explanations of the unique characteristics associated with these solutions.

In various works [29–32], researchers have explored the extension of spherically symmetric BHs to higher dimensions using a nonlinear Lagrangian that focuses on the power of the Maxwell invariants. These studies delve into the generalization of such BHs in a broader context. In the rotating version of Einstein–Born–Infeld model, black branes and black strings [26,33,34] have been studied. An effective Lagrangian Heisenberg–Euler–Schwinger model for nonlinear electromagnetic fields was developed. Heisenberg and Euler implemented the theory of a Dirac electron–positron for the first time [20]. Schwinger recasted the nonperturbative single loop effective Lagrangian in quantum electrodynamics (QED) [35]. When the strength of electric fields is greater, the value of threshold energy of vacuum $E_c = \frac{m^2c^3}{eh}$ can be reduced by the spontaneous formation of pairs of electron and positron [20,35,36]. For decades, researchers have become fascinated by the creation of pairs of electrons and positrons from the vacuum of quantum electrodynamics (QED) and the polarization of the vacuum by an outside electromagnetic field (Refs. [37,38]). QED is basic framework that describes electromagnetic interactions and has been demonstrated through experiments. It is crucial to investigate QED implications in physics of BH.

The structure of this paper is as: In Section 2, we study the review of Einstein–Euler–Heisenberg BH. Section 3 analyses the motion of massive as well as massless particles, including it is effective potential, applying the unified Einstein–Euler–Heisenberg theory. The focus of this section includes examining structure of horizon, and orbits of photons, and radius of the inner circular orbit (ISCO) of massive particles orbiting around the BHs enriched with electric and magnetic charges. It is demonstrated that magnetic and electric fields of spherically symmetric BH do not vanish. Then, Section 4 delves deeper into the gravitational weak lensing phenomenon. A comprehensive approach is employed to investigate this phenomenon and explore the deflection angle of light rays near magnetically and electrically charged BH. In the last section, we conclude our findings of the study.

2. Black Holes in Einstein–Euler–Heisenberg (EEH) Theory

The EEH theory's action incorporates the Einstein–Hilbert action with an added term that corresponds to a forcible electromagnetic field. This field is characterized by its invariants F and G, which are functions $F_{\mu\nu}$ and $F^{\mu\nu}$. The EEH theory's action describes dynamics of the electromagnetic and gravitational fields. This is an integral over the spacetime of Lagrangian density that is a function of fields and their derivatives. EEH action from [39] is expressed as

$$S = \frac{1}{4\pi}\int d^4x\sqrt{-g}\left(\frac{1}{4}R - \mathcal{L}(F,G)\right), \tag{1}$$

where $L(F,G)$ refers to the functional of $F = \frac{1}{4}F_{\mu\nu}F^{\mu\nu}$ and $G = \frac{1}{4}F^{\mu\nu}F^{*}_{\mu\nu}$ with strength of electromagnetic field $F_{\mu\nu}$ and $F^{*}_{\mu\nu} = \frac{1}{2}\epsilon_{\mu\nu\sigma\rho}F^{\sigma\rho}$. The Levi-Civita tensor satisfies $\epsilon_{\mu\nu\sigma\rho}\epsilon^{\mu\nu\sigma\rho} = -4!$. As single-loop corrections to quantum electrodynamics (QED), the Lagrangian of Euler–Heisenberg is

$$\mathcal{L}(F,G) = -F + \frac{1}{2}F^2 + \frac{7a}{8}G^2, \tag{2}$$

where a is the coupling constant [20,21]. Two frameworks are important nonlinear electrodynamics. One is the P framework constructed by the tensor $P_{\mu\nu}$, and the other is framework F constructed by the electromagnetic field tensor $F_{\mu\nu}$. P is defined by

$$P_{\mu\nu} = (1 - aF)F_{\mu\nu} - \frac{7a}{4}F^{*}_{\mu\nu}G. \tag{3}$$

Einstein–Euler–Heisenberg theory predicts the spherically symmetric spacetime given as follows in spherical polar coordinates [21]:

$$ds^2 = -f(r)\,dt^2 + \frac{dr^2}{f(r)} + r^2(d\theta^2 + \sin^2\theta\, d\Phi^2), \tag{4}$$

where

$$f(r) = 1 - \frac{2GM}{r} + \frac{GQ^2}{4\pi r^2} + \frac{GQ_m^2}{4\pi r^2}. \tag{5}$$

where Q is electric charge and Q_m is magnetic charge. Using the Einstein–Euler–Heisenberg BH solution taking $f(r) = 0$, we can evaluate the event horizon of BH, as shown in Figure 1. One can notice that the event horizon decreases by increasing the electric and magnetic charge.

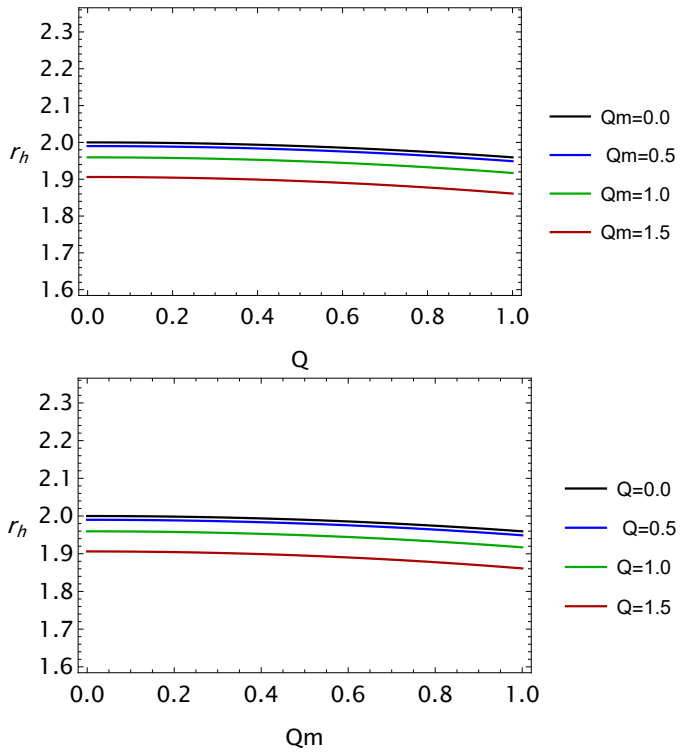

Figure 1. Relation of radius event horizon r_h and parameters Q and Q_m for black hole. We set M = 1.

3. Particle Dynamics Around Black Hole in EEH Theory

Within this section, we investigated the dynamics of massless and massive particles orbiting within framework of EEH BH.

3.1. Massive Particle Motions Orbiting Black Holes in EEH Theory

First, we investigate the movement of massive particles typically orbiting around the Einstein–Euler–Heisenberg BH. To determine the orbits of a test particle with mass m, consider the Lagrangian of the EEH BH in the following form:

$$\mathcal{L}' = \frac{1}{2} g_{\mu\nu} u^\mu u^\nu \quad , \quad u^\mu = \frac{dx^\mu}{d\tau}. \tag{6}$$

where the affine parameter is abbreviated by τ, four velocity and coordinates of the test particle are expressed by u^μ and x^μ, respectively. Also, we can write energy "ε" and angular momentum "$\mathcal{L}$" for the test particle as

$$\varepsilon = \frac{\partial L'}{\partial \mu'} = -f(r)\frac{dt}{d\tau}, \tag{7}$$

$$\mathcal{L} = \frac{\partial L'}{\partial \mu^\phi} = r^2 \sin^2\theta \frac{d\theta}{d\tau}, \tag{8}$$

By substituting the expressions in Equation (8) and using the condition $g_{\mu\nu} u^\mu u^\nu = -\epsilon$ one may obtain an expression representing the test particle's motion in the following structure:

$$\frac{d\theta}{d\tau} = \frac{1}{r^2}\sqrt{\kappa - \frac{\mathcal{L}^2}{\sin^2\theta}}, \tag{9}$$

$$\frac{d\Phi}{d\tau} = \frac{\mathcal{L}^2}{r^2 \sin^2\theta}, \tag{10}$$

$$\frac{dt}{d\tau} = \frac{\varepsilon}{f(r)}, \tag{11}$$

where κ represents the Carter constant, and the parameter ε is defined as follows:

$$\epsilon = \begin{cases} 1, & \text{for timelike geodesic} \\ 0, & \text{for null geodesics} \\ -1, & \text{for spacelike geodesics} \end{cases} \tag{12}$$

For the purpose of simplicity, we consider the velocity of particle's is in the equatorial plan that meets the criteria $\frac{d\theta}{d\tau} = 0$ and $\theta = \frac{\pi}{2}$. In this particular case, $\kappa = \mathcal{L}^2$, and equation representing radial motion will be in the following form:

$$\left(\frac{dr}{dt}\right)^2 = \varepsilon^2 - v_{\text{eff}}(r) = \varepsilon^2 - f(r)\left(1 + \frac{\mathcal{L}^2}{r^2}\right), \tag{13}$$

$$V_{\text{eff}} = f(r)\left(1 + \frac{\mathcal{L}^2}{r^2}\right). \tag{14}$$

The relationship of radial coordinates and effective potential for massive test particles near BH for various values of Q and Q_m parameters is represented in Figure 2. It can be noted that these parameters have a potential impact on the effective potential. Graphs show that with an increase in values of parameter Q, stable circular orbits start moving towards BH's center, while parameter Q_m also has the same effect.

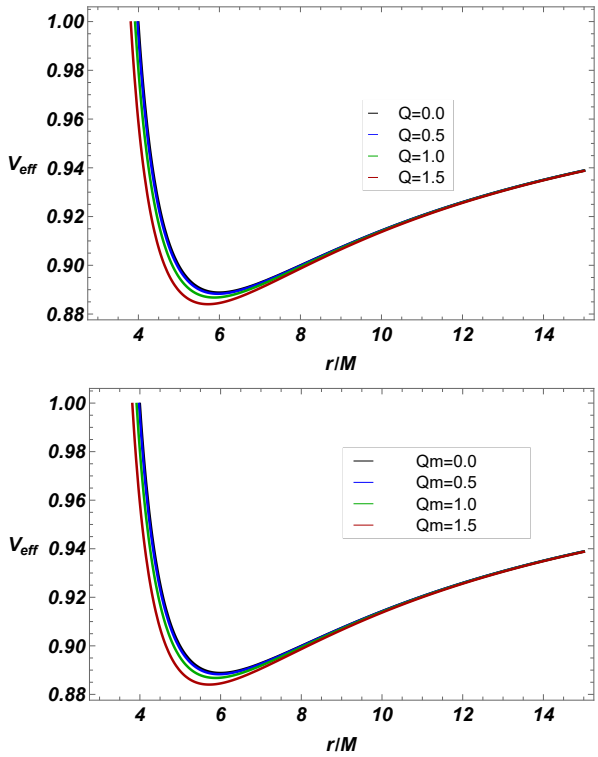

Figure 2. Relation of V_{eff} and massive particle's radial coordinate r with variation in parameters Q and Q_m.

To calculate the circular motion of the neutral particle around BH, we apply the ahead-stated conditions $\dot{r} = 0$ and $\ddot{r} = 0$. Application of these conditions will give formulas for $\mathcal{L}$ and ϵ for test particles, given as

$$\mathcal{L}^2 = \frac{r^2(GQ^2 - 4GM\pi r + GQ_m^2)}{2(GQ^2 + 2\pi r(-3GM + r)GQ_m^2)}, \tag{15}$$

and

$$\varepsilon^2 = \frac{(GQ^2 + 4\pi r(-2GM + r) + GQ_m^2)^2}{8\pi r^2(GQ^2 + 2\pi r(-3GM + r) + GQ_m^2)}. \tag{16}$$

Plotting these conservative quantities can provide the readers with an additional information, as can be seen in Figures 3 and 4. These graphs show that the increase in parameters Q and Q_m shifts the radial coordinates towards the center.

Now, we will examine the *ISCO* radius r_{ISCO}. To find the *ISCO* radius, we will utilize the following conditions:

$$\begin{cases} V'_{\text{eff}} = 0, \\ V''_{\text{eff}} = 0, \end{cases} \tag{17}$$

With the complicated nature of effective potential, we cannot acquire a precise analytical expression for r_{ISCO}. However, we can plot *ISCO* radius directly without explicitly solving it, as shown in Figure 5. Based on Figure 5, one can obtain information about dependence of *ISCO* radius for different values of Q and Q_m EEH BH. *ISCO* radius falls as the parameters Q and Q_m increase.

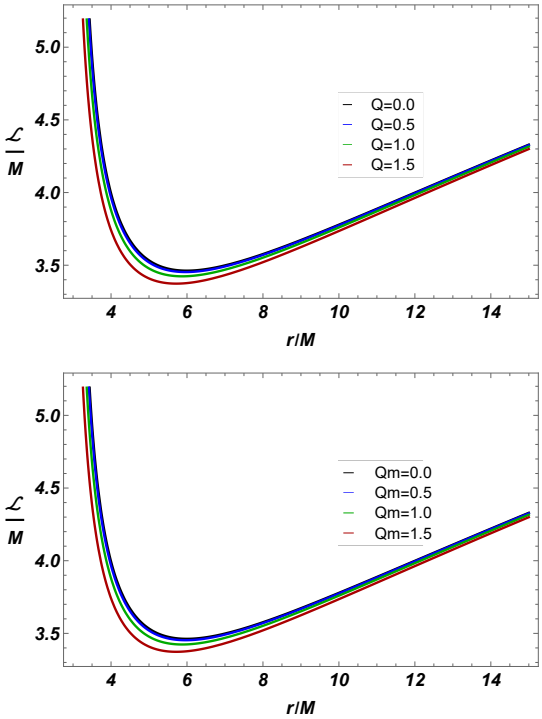

Figure 3. Relation between angular momentum $\frac{\mathcal{L}}{M}$ and radial coordinates for different values of Q_m and Q.

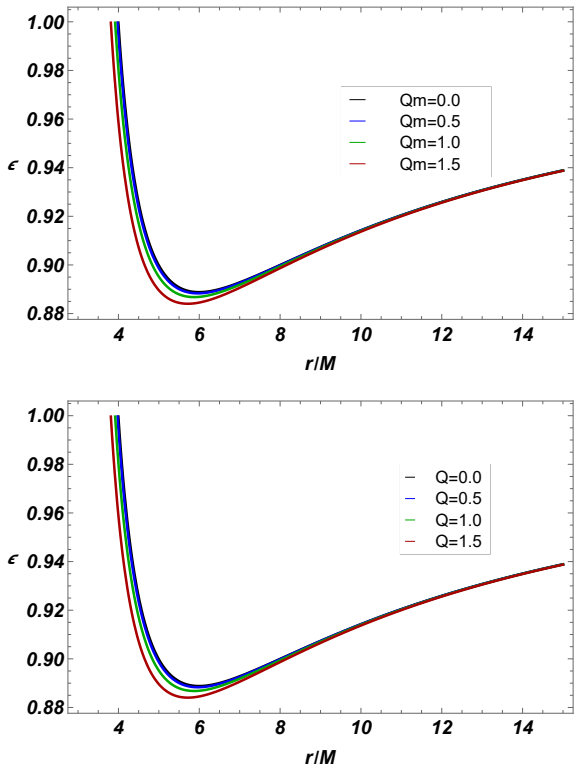

Figure 4. Relation between ϵ and radial coordinates for different Q and Q_m values.

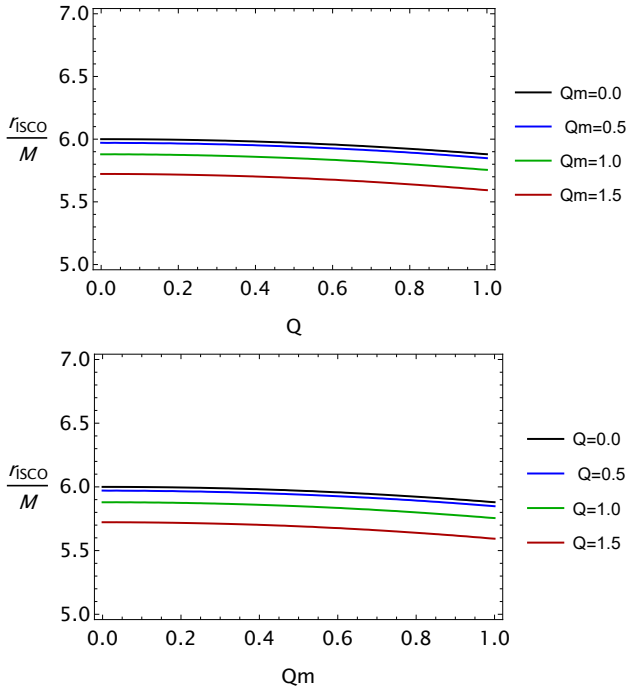

Figure 5. Relation of $\frac{r_{ISCO}}{M}$ and parameters Q and Q_m.

3.2. Motion of Massless Particles (Photon)

In this section, we analyze the motion of photon (massless) particles around EEH BH spacetime. Using Lagrangian (6), we put $\epsilon = 0$ in Equation (12) to derive the equation of photon motion orbiting the BH and at equatorial plane, which can be expressed as

$$\dot{r}^2 = \varepsilon^2 - f(r)\frac{\mathcal{L}^2}{r^2}, \tag{18}$$

$$\dot{\phi} = \frac{\mathcal{L}}{r^2}, \tag{19}$$

$$\dot{t} = \frac{\varepsilon}{f(r)}, \tag{20}$$

Utilizing Equation (18), we will have an expression for effective potential V_{eff} for photon's radial motion,

$$V_{\text{eff}} = f(r)\frac{\mathcal{L}^2}{r^2}, \tag{21}$$

Figure 6, displays the relation between effective potential and radial coordinates for different values of electric charge Q and magnetic charge Q_m. Graphs reveal that the Q and Q_m parameters cause photon orbits to move towards the center of BH.

The photon's orbit radius r_{ph} orbiting around BH is the result of the solution to the following equation:

$$V'_{\text{eff}} = 0, \tag{22}$$

which will give us expression for r_{ph}, written as:

$$r_{ph} = \frac{2GM\pi - \sqrt{\pi}\sqrt{-GQ^2 + 4GM^2\pi - G(Q_m)^2}}{2\pi}. \tag{23}$$

The relationship between photon orbit's radius r_{ph} and the EEH BH parameters Q and Q_m is graphed in Figure 7. An increase in parameters Q and Q_m causes a decrease in the photon's orbit radius.

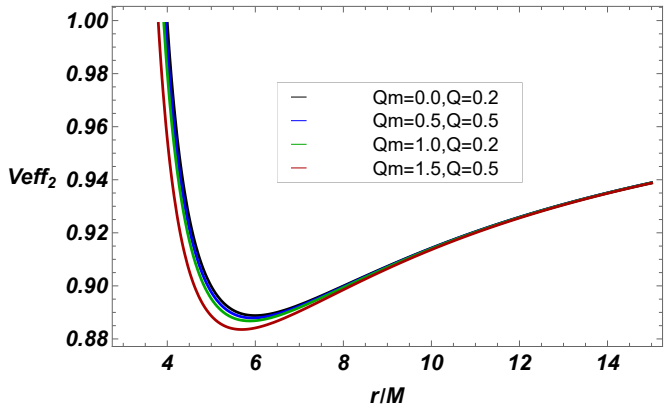

Figure 6. Relations between V_{eff} and radial coordinates for the different values of black hole parameters Q and Q_m.

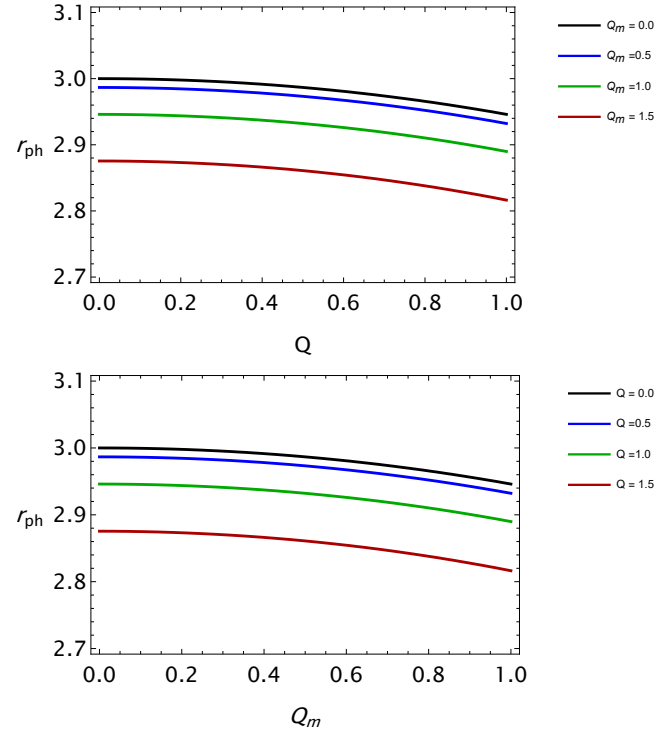

Figure 7. Relations between radius of photon r_{ph} and parameters Q_m and Q.

4. Weak Gravitational Lensing in Einstein–Euler–Heisenberg Theory

This part examines the optical properties of EEH BH utilizing the weak gravitational lensing phenomenon. We use following notation of metric tensor for approximation of weak field [40,41]:

$$g_{\alpha\beta} = \eta_{\alpha\beta} + h_{\alpha\beta}, \tag{24}$$

where $h_{\alpha\beta}$ and $\eta_{\alpha\beta}$ are expressions for perturbation gravity field and Minkowshki spacetime describing EEH theory, respectively. One must have to consider the following properties for $\eta_{\alpha\beta}$ and $h_{\alpha\beta}$:

$$\eta_{\alpha\beta} = diag(-1, 1, 1, 1)$$

$$under \quad x^{\alpha} \to \infty, \quad h_{\alpha\beta} \to 0, \quad h_{\alpha\beta} << 1,$$
$$h^{\alpha\beta} = h_{\alpha\beta}, \quad g^{\alpha\beta} = \eta^{\alpha\beta} - h^{\alpha\beta}. \tag{25}$$

In this part, we studied the optical properties of EEH BH using weak gravitational lensing effects. For weak field approximation, we consider the metric tensor's notation as used in references [31,35]. Utilizing the basic equations, we will obtain the expression for angle of deflection for EEH theory, given as follows [31]:

$$\alpha_b = \int_0^\infty \frac{b}{r}\left(\partial_r(h_{33}) + \frac{1}{1-\frac{w_e^2}{w}}\partial_r(h_{\theta\theta}) - \frac{k_e}{w^2-w_e^2}(\partial_r N)\right)dz, \tag{26}$$

where ω_θ and ω are quantities representing plasma frequencies and photon frequencies, respectively. One can rewrite the line element from Equation (4) in the following form:

$$\begin{aligned} ds^2 =& ds_\theta + \left(\frac{R_s G}{r} - \frac{GQ^2}{4\pi r^2} - \frac{GQ_m^2}{4\pi r^2}\right)dt^2 \\ &+ \left(\frac{R_s G}{r} - \frac{GQ^2}{4\pi r^2} - \frac{GQ_m^2}{4\pi r^2}\right)dr^2, \end{aligned} \tag{27}$$

where

$$ds_\theta = -dt^2 + dr^2 + (d\theta^2 + \sin[\theta']^2 d\Phi^2)$$

$$h_{\theta\theta} = \frac{G}{r}\left(R_s - \frac{1}{4\pi r}(Q^2 - Q_m^2)\right) \tag{28}$$

$$h_{ij} = \frac{G}{r}\left(R_s - \frac{1}{4\pi r^2}(Q^2 - Q_m^2)\right)n_i n_j, \tag{29}$$

$$h_{33} = \frac{G}{r}\left(R_s - \frac{1}{4\pi r^2}(Q^2 - Q_m^2)\right)\cos^2\chi, \tag{30}$$

where $\cos^2\chi = z^2/(b^2+z^2)$ and $r^2 = b^2 + z^2$. The derivatives of h_{00} and h_{33} by radial coordinate are defined as:

$$\frac{d}{dr}(h_{\theta\theta}) = \frac{GQ^2}{2\pi r^3} + \frac{GQ_m^2}{2\pi r^3} - \frac{GR_s}{r^2}, \tag{31}$$

$$\frac{d}{dr}(h_{33}) = \frac{Z^2(GQ^2 + GQ_m^2 - 3G\pi r R_s)}{\pi r^5}, \tag{32}$$

and one can write the mathematical form for angle of deflection [42] as:

$$\hat{\alpha} = \hat{\alpha_1} + \hat{\alpha_2} + \hat{\alpha_3}, \tag{33}$$

with

$$\begin{aligned} \hat{\alpha_1} &= \frac{1}{2}\int_{-\infty}^{\infty}\frac{b}{r}\frac{dh_{33}}{dr}dz, \\ \hat{\alpha_2} &= \frac{1}{2}\int_{-\infty}^{\infty}\frac{b}{r}\frac{1}{1-\frac{w_e^2}{w}}\frac{dh_{00}}{dr}dz, \\ \hat{\alpha_3} &= \frac{1}{2}\int_{-\infty}^{\infty}\frac{b}{r}\left(-\frac{K_e}{w^2-w_e^2}\right)\frac{dN}{dr}dz, \end{aligned} \tag{34}$$

Our objective is to investigate the angle of deflection for different distributions of plasma density.

4.1. Case 1: In Presence of Uniform Plasma

The deflection angle of EEH BH with uniform plasma may be expressed as [42]:

$$\alpha_{\text{uni}} = \alpha_{\text{uni1}} + \alpha_{\text{uni2}} + \alpha_{\text{uni3}} \tag{35}$$

Using Equations (30), (33), and (34), one will be able to find the expression for the deflection angle in the presence of a homogeneous plasma around BH:

$$\alpha_{\text{uni}} = \frac{GQ^2}{16b^2} + \frac{GQ_m^2}{16b^2} - \frac{GR_s}{b} + \left(\frac{GQ^2}{8b^2} + \frac{GQ_m^2}{8b^2} - \frac{GR_s}{b}\right)\frac{w^2}{w^2 - w_e^2}, \tag{36}$$

Using the equation above, we can illustrate the relation between the deflection angle and impact parameter b for different values of parameters Q_m, Q ,and w_e^2/w^2, as illustrated in Figure 8. We also investigated the relationship between deflection angle and plasma parameters By varying BH parameters Q and Q_m, as shown in Figures 8–11.

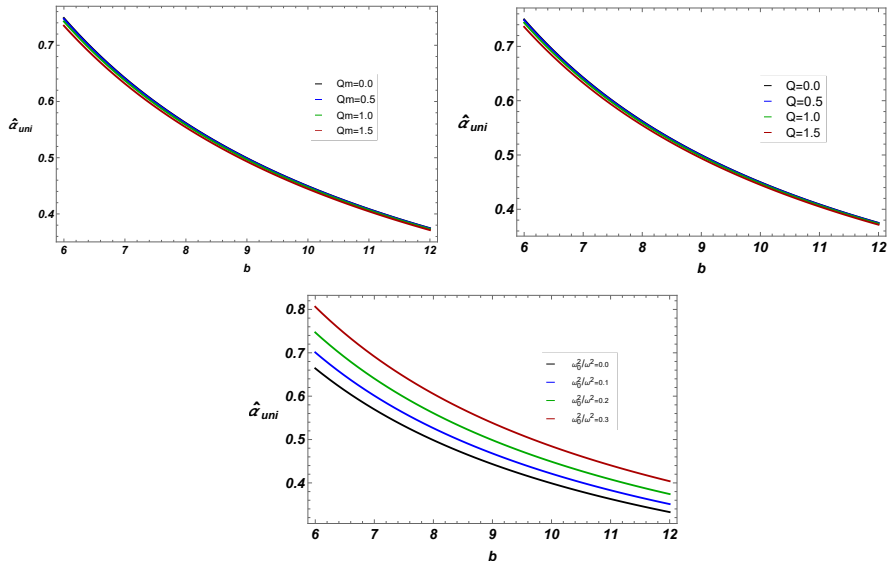

Figure 8. Relation between uniform deflection angle $\hat{\alpha}_{uni}$ and impact parameter with the variation in parameters Q, Q_m, and w_e^2/w^2.

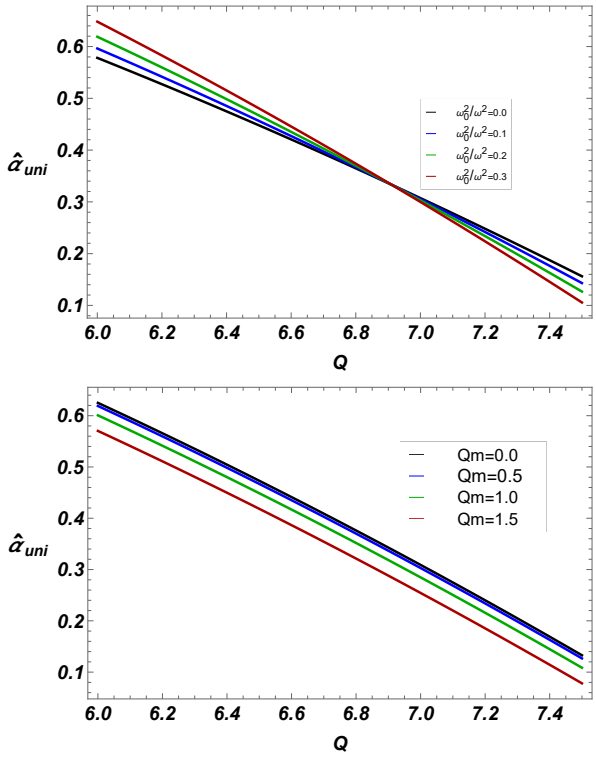

Figure 9. Relation between uniform deflection angle $\hat{\alpha}_{uni}$ and parameter Q with the variation in parameters Q_m and w_e^2/w^2; here, $b = 3$ is fixed.

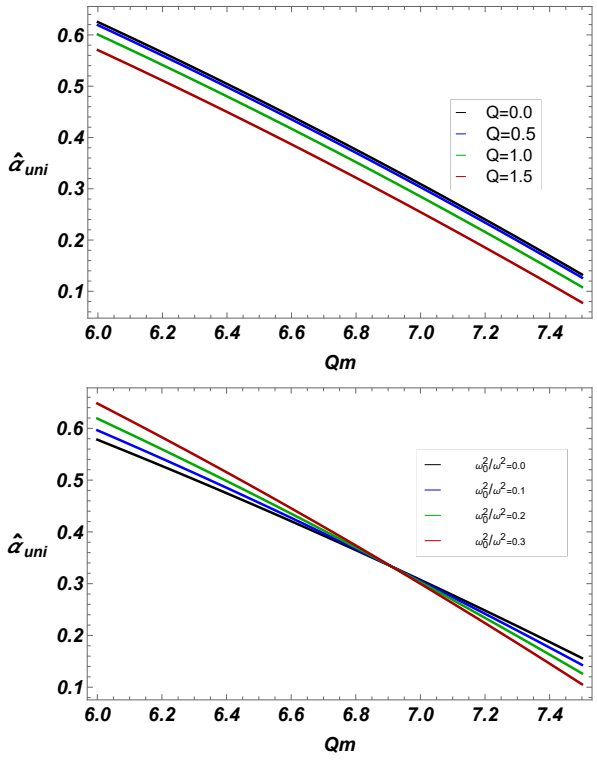

Figure 10. Relation between uniform deflection angle $\hat{\alpha}_{uni}$ and parameter Q_m with the variation in parameters Q and w_e^2/w^2; here, $b = 3$ is fixed.

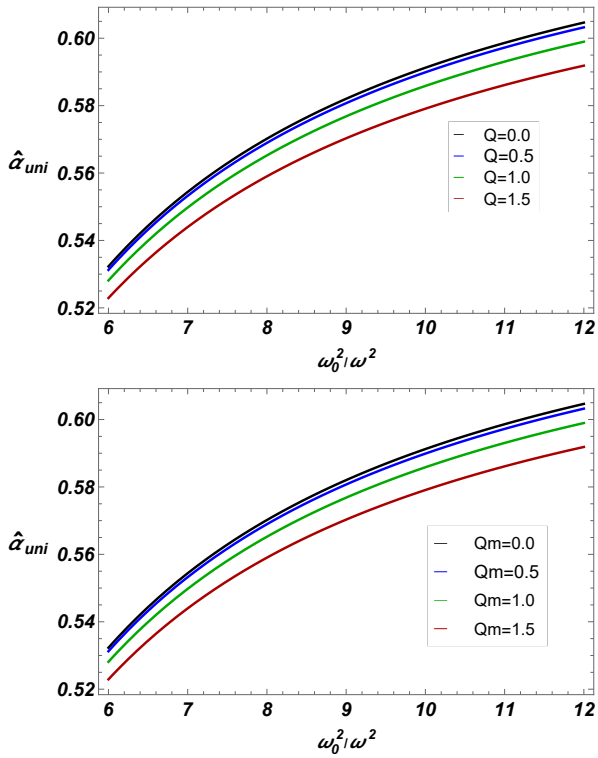

Figure 11. Relation between uniform deflection angle $\hat{\alpha}_{uni}$ and w_e^2/w^2 with the variation in parameters Q_m and Q; here, $b = 3$ is fixed.

4.2. Case 2: In the Presence of Non-Uniform Plasma

Based on our study, a model depicting a non-singular isothermal sphere (SIS) with a singularity at it is center appears to be the most suitable for comprehending the unique behaviors exhibited by photons that experience weak gravitational lensing in the surround-

ings of BHs. An SIS is cloud of gas in a spherical shape, featuring a singularity located at the center of the spherical shape where density becomes extremely high. The density distribution of the SIS plasma field is stated in [40], as given below:

$$\rho(r) = \frac{\sigma_v^2}{2\pi r^2}, \tag{37}$$

where σ_v^2 represents uni-dimensional dispersion of velocity. Concentrations of plasma allows us to have the following analytical expression:

$$N(r) = \frac{\rho(r)}{km_p}, \tag{38}$$

where k is a constant coefficient, which is dimensionless and m_p is proton mass. So, we have an expression for the frequency of plasma as:

$$w_e^2 = K_e N(r) = \frac{K_e \sigma_v^2}{2\pi k m_p r^2}. \tag{39}$$

Now, we investigate the influence of SIS plasma on deflection angle. One can have an expression for deflection angle in SIS plasma field as follows [41]:

$$\hat{\alpha}_{SIS} = \hat{\alpha}_{SIS1} + \hat{\alpha}_{SIS2} + \hat{\alpha}_{SIS3}. \tag{40}$$

By combining Equations (30), (34), and (40), we can obtain deflection angle in the following expression:

$$\hat{\alpha}_{SIS} = \frac{3GQ^2}{16b^2} + \frac{3GQ_m^2}{16b^2} - \frac{2GR_s}{b} - \frac{R_s^2 w_c^2}{2b^2 w^2} + \frac{3GQ^2\sigma^2 K_e}{64b^4 km\pi w^2} + \frac{3GQ_m^2\sigma^2 K_e}{64b^4 km\pi w^2} - \frac{G\sigma^2 K_e R_s^2}{3b^3 km\pi w^2}. \tag{41}$$

From [43], we have:

$$w_e^2 = \frac{K_e \sigma_v^2}{2\pi k m_p R_s^2}. \tag{42}$$

Utilizing Equation (41), we have illustrated the relation of deflection angle and impact parameter b for different choices for values of Q, Q_m, and w_e^2/w^2. Figure 12 depicts deflection angle in non-uniform plasma medium using EEH BH solution. In Figures 12 and 13, we show how a non-uniform plasma affects the angle of deflection of the beam of light near BH. Furthermore, we investigated impacts of plasma parameter on deflection angle as shown in Figures 14 and 15.

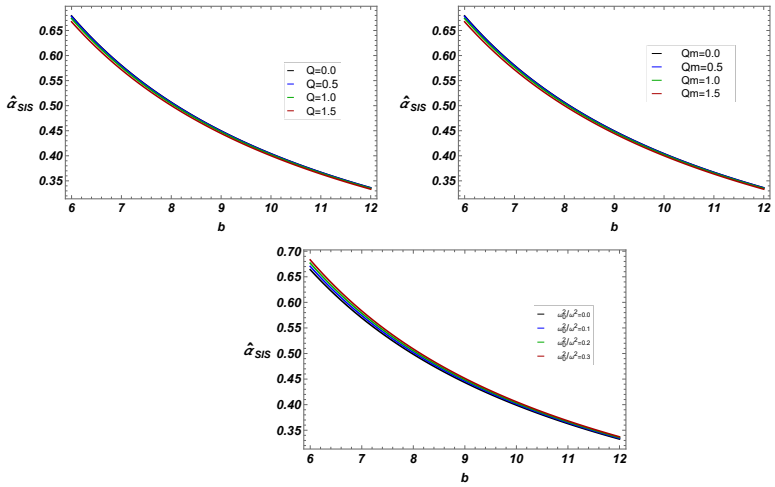

Figure 12. Relation between SIS plasma deflection angle $\hat{\alpha}_{SIS}$ and impact parameter b for the variation in parameters Q, Q_m, and w_e^2/w^2.

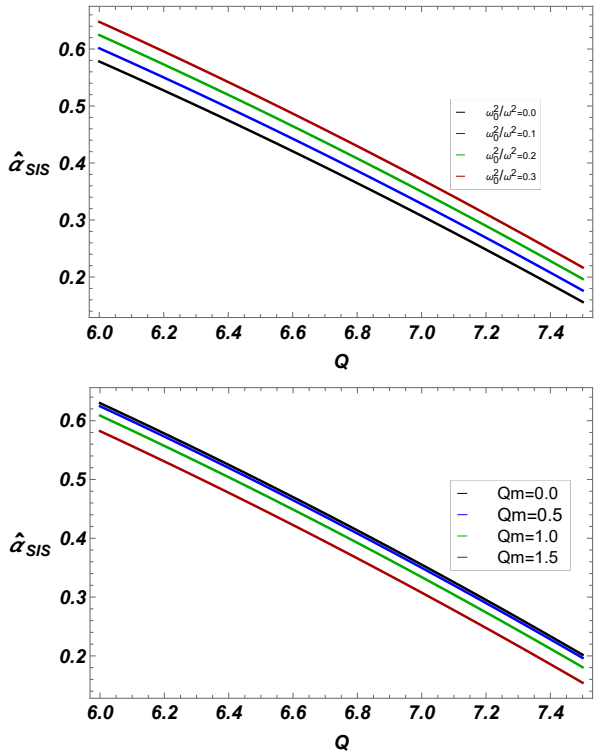

Figure 13. Relation between SIS plasma deflection angle $\hat{\alpha}_{SIS}$ and parameter Q for variation in parameters Q_m and w_e^2/w^2; here, $b = 3$ is fixed.

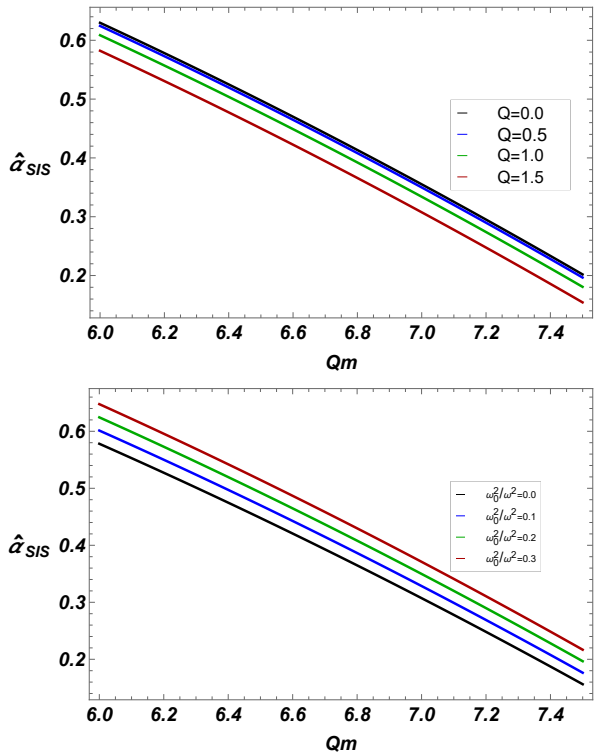

Figure 14. Relation between SIS plasma deflection angle $\hat{\alpha}_{SIS}$ and parameter Q_m for variation in parameters Q and w_e^2/w^2; here, $b = 3$ is fixed.

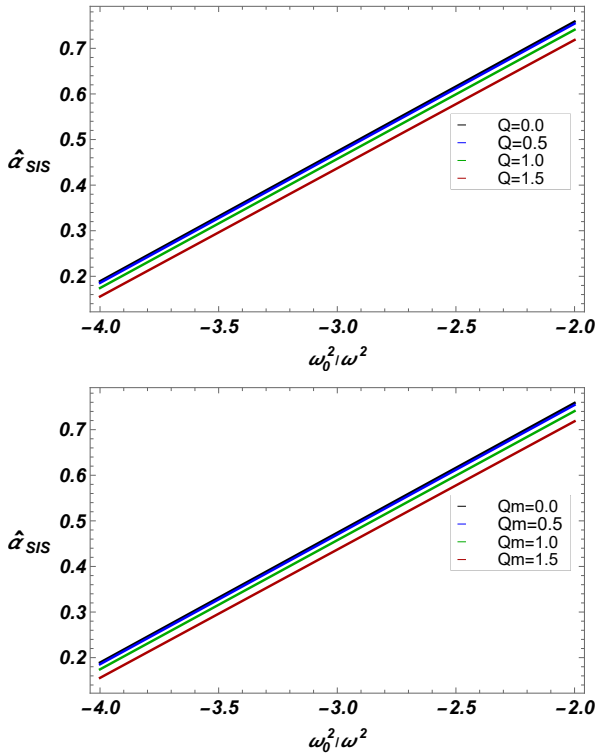

Figure 15. Relation SIS plasma deflection angle $\hat{\alpha}_{SIS}$ and w_e^2/w^2 with the variation in parameters Q_m and Q; here, $b = 3$ is fixed.

5. Comparison

Comparison of deflection angles in both cases is illustrated by Figure 16. Our work shows that for the given fixed BH parameters in the case of EEH BH, uniform plasma has a higher impact on deflection angle than non-uniform plasma.

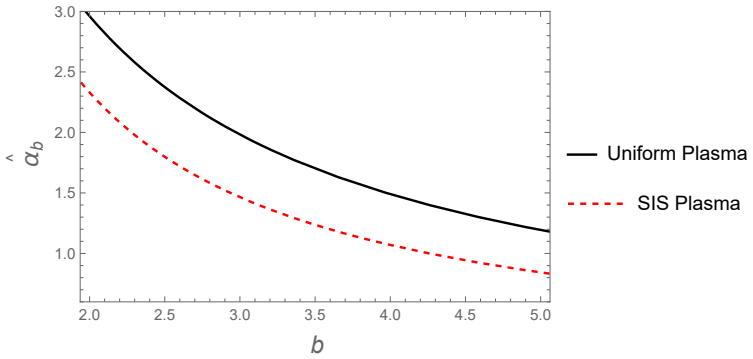

Figure 16. Comparison of angle of deflection in both cases.

6. Summary

This article explores the role of the effective Lagrangian of Euler–Heisenberg in developing Einstein–Euler–Heisenberg BH solution, alongside the Maxwell Lagrangian. Within this study, we have explored the optical characteristics of BH in EEH theory for massless and massive particles, and also, we discussed weak gravitational lensing. If we replace $Q^2 + Q_m^2 \to Q^2$ in Equation (5), we will obtain the BH solution that coincides with the four-dimensional Reissner–Nordström (RN) one with the charge Q. Some similar works have been obtained regarding RN-like BH solutions in the literature [43–47]. However, our BH solution is different one, as it contains two charges, the electric charge Q and magnetic charge Q_m, instead of single charge Q, which is not addressed in RN solutions. In this study,

we analyzed the the individual effect these charges instead of combined effect. Additionally, we integrate quantum electrodynamics corrections that introduce screening effects for electric charges and paramagnetic effects for magnetic charges, resulting in novel physical insights. In contrast to prior investigations of RN black holes, our analysis delineates the individual and synergistic effects of Q and Q_m on effective potential, photon orbits, inner circular orbits, and weak gravitational lensing, revealing substantial differences and new outcomes attributable to the EEH framework. These results enhance our comprehension of BH physics and underscore the distinctive contributions of EEH theory. Our results summary is as follows:

- We worked on BH's horizon structure using the effective Lagrangian of EEH BH solution. The findings show that increasing the parameter Q and Q_m decreases the event horizon radius, as shown in Figure 1.
- We discussed the particle motion effective potential near BH. We investigated the relation between massive and massless particle effective potential along radial coordinate r for various values of EEH BH parameters Q and Q_m. We noticed that effective potential decreases by increasing these parameters.
- We explored the ISCO radius for massive particles surrounding BH. It has been shown that with an increases in the values of EEH BH parameters Q and Q_m, the ISCO radius decreases (see Figure 5).
- The photon's sphere radius is also studied near BH using the effective Lagrangian of EEH BH. Photon orbits decrease with increase in BH parameters, as shown in Figure 7.
- We have also studied deflection angle near EEH BH with plasma (homogeneous, and non-homogeneous fields). Our work shows that for fixed BH parameters, uniform plasma has the greater impact on deflection angle than non-uniform plasma.

This study's findings reveal new opportunities for investigating the interaction between electric and magnetic charges in BH physics, especially considering quantum electrodynamics corrections. Subsequent research may expand upon this study by examining the thermodynamic features, performing stability analyses, and exploring potential observational signatures of BHs within the Einstein–Euler–Heisenberg framework, so enhancing our understanding of the quantum characteristics of gravity and electromagnetism.

Author Contributions: The authors in this manuscript contributed as: A.D.: Supervised the project and prepared revisions of the manuscript. R.S.M.: Supervised the project and contributed to the draft writing. M.F.: Performed formal analysis and software use. B.B.: Performed formal analysis and prepared the original draft. S.D.: Performed formal analysis and prepared the original draft. R.J.: Performed formal analysis and prepared the original draft. A.M.: Proofread and prepared the final draft of the article. All authors have read and agreed to the published version of the manuscript.

Funding: This project has no available funding.

Data Availability Statement: This study is theoretical and contains no observational or associated data.

Acknowledgments: Asif Mahmood would like to acknowledge Researcher's Supporting Project Number (RSP2025R43), King Saud University, Riyadh, Saudi Arabia.

Conflicts of Interest: Authors in this study are attached due to research work and have no conflicts of interest.

References

1. Abbott, B.P.; Abbott, R.; Abbott, T.D.; Abernathy, M.R.; Acernese, F.; Ackley, K.; Adams, C.; Adams, T.; Addesso, P.; Addesso, P.; et al. Observation of Gravitational Waves from a Binary Black Hole Merger. *Phys. Rev. Lett.* **2016**, *116*, 061102. arXiv:1602.03837. [CrossRef] [PubMed]

2. Akiyama, K.; Alberdi, A.; Alef, W.; Asada, K.; Azulay, R.; Baczko, A.K.; Ball, D.; Baloković, M.; Barrett, J.; Bintley, D.; et al. First M87 event horizon telescope results. VI. The shadow and mass of the central black hole. *Astrophys. J. Lett.* **2019**, *875*, L6. [CrossRef]
3. Will, C.M. The confrontation between general relativity and experiment. *Living Rev. Relativ.* **2014**, *17*, 4. [CrossRef]
4. Born, M.; Infeld, L. Foundations of the new field theory. *Proc. R. Soc. A* **1934**, *144*, 425–451. [CrossRef]
5. Hoffmann, B. Gravitational and electromagnetic mass in the Born-Infeld electrodynamics. *Phys. Rev.* **1935**, *47*, 877–880. [CrossRef]
6. Hoffmann, B.; Infeld, L. On the choice of the action function in the new field theory. *Phys. Rev.* **1937**, *51*, 765–773. [CrossRef]
7. Fradkin, E.S.; Tseytlin, A.A. Non-linear electrodynamics from quantized strings. *Phys. Lett. B* **1985**, *163*, 123–130. [CrossRef]
8. Abouelsaood, A.; Callan, C.G.; Nappi, C.R.; Yost, S.A. Open strings in background gauge fields. *Nucl. Phys. B* **1987**, *280*, 599–624. [CrossRef]
9. Tseytlin, A.A. On non-abelian generalisation of the Born-Infeld action in string theory. *Nucl. Phys. B* **1997**, *501*, 41–52. [CrossRef]
10. Garcia, A.; Salazar, H.; Plebanski, J.F. Type-D solutions of the Einstein and Born-Infeld nonlinear-electrodynamics equations. *Il Nuovo C. B* **1984**, *84*, 65–90. [CrossRef]
11. Demianski, M. Static electromagnetic geon. *Found. Phys.* **1986**, *16*, 187–190. [CrossRef]
12. Fernando, S.; Krug, D. Charged black hole solutions in Einstein-Born-Infeld gravity with a cosmological constant. *Gen. Relativ. Gravit.* **2003**, *35*, 129–137. [CrossRef]
13. Dey, T.K. Born–Infeld black holes in the presence of a cosmological constant. *Phys. Lett. B* **2004**, *595*, 484–490.
14. Diaz-Alonso, J.; Rubiera-Garcia, D. Electrostatic spherically symmetric configurations in gravitating nonlinear electrodynamics. *Phys. Rev. D* **2010**, *81*, 064021. [CrossRef]
15. Diaz-Alonso, J.; Rubiera-Garcia, D. Asymptotically anomalous black hole configurations in gravitating nonlinear electrodynamics. *Phys. Rev. D* **2010**, *82*, 085024. [CrossRef]
16. Diaz-Alonso, J.; Rubiera-Garcia, D. Black holes from generalized gauge field theories. *J. Phys. Conf. Ser.* **2011**, *283*, 012014. [CrossRef]
17. Diaz-Alonso, J.; Rubiera-Garcia, D. Electrically charged black hole solutions in generalized gauge field theories. *J. Phys. Conf. Ser.* **2011**, *314*, 012065. [CrossRef]
18. Soleng, H.H. Charged black points in general relativity coupled to the logarithmic U (1) gauge theory. *Phys. Rev. D* **1995**, *52*, 6178–6181. [CrossRef] [PubMed]
19. de Oliveira, H.P. Non-linear charged black holes. *Class. Quantum Gravity* **1994**, *11*, 1469–1482. [CrossRef]
20. Heisenberg, W.; Euler, H. Folgerungen aus der diracschen theorie des positrons. *Z. Phys.* **1936**, *98*, 714–732. [CrossRef]
21. Yajima, H.; Tamaki, T. Black hole solutions in Euler-Heisenberg theory. *Phys. Rev. D* **2001**, *63*, 064007. [CrossRef]
22. Ayón-Beato, E.; García, A. Regular black hole in general relativity coupled to nonlinear electrodynamics. *Phys. Rev. Lett.* **1998**, *80*, 5056–5059. [CrossRef]
23. Ayón-Beato, E.; García, A. New regular black hole solution from nonlinear electrodynamics. *Phys. Lett. B* **1999**, *464*, 25–29. [CrossRef]
24. Cirilo Lombardo, D.J. Charge without charge, regular spherically symmetric solutions and the Einstein-Born-Infeld theory. *Int. J. Theor. Phys.* **2009**, *48*, 2267–2285. [CrossRef]
25. Burinskii, A.; Hildebrandt, S.R. New type of regular black holes and particlelike solutions from nonlinear electrodynamics. *Phys. Rev. D* **2002**, *65*, 104017. [CrossRef]
26. Hendi, S.H. Rotating black string with nonlinear source. *Phys. Rev. D* **2010**, *82*, 064040. [CrossRef]
27. Novello, M.; Bergliaffa, S.E.P.; Salim, J.M. Singularities in general relativity coupled to nonlinear electrodynamics. *Class. Quantum Gravity* **2000**, *17*, 3821–3832. [CrossRef]
28. Bronnikov, K.A. Regular magnetic black holes and monopoles from nonlinear electrodynamics. *Phys. Rev. D* **2001**, *63*, 044005. [CrossRef]
29. Hassaïne, M.; Martínez, C. Higher-dimensional black holes with a conformally invariant Maxwell source. *Phys. Rev. D* **2007**, *75*, 027502. [CrossRef]
30. Hassaïne, M.; Martínez, C. Higher-dimensional charged black hole solutions with a nonlinear electrodynamics source. *Class. Quantum Gravity* **2008**, *25*, 195023. [CrossRef]
31. González, H.A.; Hassaïne, M.; Martínez, C. Thermodynamics of charged black holes with a nonlinear electrodynamics source. *Phys. Rev. D* **2009**, *80*, 104008. [CrossRef]
32. Mazharimousavi, S.H.; Halilsoy, M.; Gurtug, O. Theorem to generate Einstein–nonlinear Maxwell fields. *Class. Quantum Gravity* **2010**, *27*, 205022. [CrossRef]
33. Dehghani, M.H.; Rastegar Sedehi, H.R. Thermodynamics of rotating black branes in $(n+1)$-dimensional Einstein-Born-Infeld gravity. *Phys. Rev. D* **2006**, *74*, 124018. [CrossRef]
34. Dehghani, M.H.; Hendi, S.H.; Sheykhi, A.; Rastegar Sedehi, H. Thermodynamics of rotating black branes in Einstein–Born–Infeld-dilaton gravity. *J. Cosmol. Astropart. Phys.* **2007**, *2*, 020. [CrossRef]

35. Schwinger, J. On gauge invariance and vacuum polarization. *Phys. Rev.* **1951**, *82*, 664–679. [CrossRef]
36. Sauter, F. On the behavior of an electron in a homogeneous electric field in Dirac's relativistic theory. *Z. Phys.* **1931**, *69*, 742–764. [CrossRef]
37. Ruffini, R.; Vereshchagin, G.; Xue, S.-S. Electron–positron pairs in physics and astrophysics: From heavy nuclei to black holes. *Phys. Rep.* **2010**, *487*, 1–140. [CrossRef]
38. Gradshteyn, I.S.; Ryzhik, I.M. *Table of Integrals, Series and Products*, 5th ed.; Academic Press: New York, NY, USA, 1994.
39. Gutiérrez, S.A.; Dudley, A.L.; Plebañski, J.F. Signals and discontinuities in general relativistic nonlinear electrodynamics. *J. Math. Phys.* **1981**, *22*, 2835–2848. [CrossRef]
40. Bisnovatyi-Kogan, G.S.; Tsupko, O.Y. Gravitational lensing in a non-uniform plasma. *Mon. Not. R. Astron. Soc.* **2010**, *404*, 1790–1800. [CrossRef]
41. Babar, G.Z.; Atamurotov, F.; Babar, A.Z. Gravitational lensing in 4-D Einstein–Gauss–Bonnet gravity in the presence of plasma. *Phys. Dark Universe* **2021**, *32*, 100798. [CrossRef]
42. Atamurotov, F.; Abdujabbarov, A.; Rayimbaev, J. Weak gravitational lensing Schwarzschild-MOG black hole in plasma. *Eur. Phys. J. C* **2021**, *81*, 118. [CrossRef]
43. Amaro, D.; Breton, N.; Lämmerzahl, C.; Macías, A. Thermodynamics of the Einstein-Euler-Heisenberg rotating black hole. *Phys. Rev. D* **2024**, *110*, 124020. [CrossRef]
44. Atamurotov, F.; Shaymatov, S.; Sheoran, P.; Siwach, S. Charged black hole in 4D Einstein-Gauss-Bonnet gravity: Particle motion, plasma effect on weak gravitational lensing and centre-of-mass energy. *J. Cosm. Astr. Phys.* **2021**, *8*, 045. [CrossRef]
45. Duan, Z.Q.; Zhao, J.Y.; Yang, K. Electrically charged black holes in gravity with a background Kalb-Ramond field. *arXiv* **2024**, arXiv:2310.13555. [CrossRef]
46. Ditta, A.; Tiecheng, X.; Atamurotov, F.; Mustafa, G.; Aripov, M.M. Particle dynamics and weak gravitational lensing around nonlinear electrodynamics black hole. *Chin. J. Phys.* **2023**, *83*, 664–679. [CrossRef]
47. Amaro, D.; Lämmerzahl, C.; Macías, A. Particle motion in the Einstein-Euler-Heisenberg rotating black hole spacetime. *Phys. Rev. D* **2023**, *107*, 084040. [CrossRef]